

Strain-Mediated Spin–Orbit Torque Enhancement in Pt/Co on Flexible Substrate

Grayson Dao Hwee Wong, Zhan Xu, Weiliang Gan, Calvin Ching Ian Ang, Wai Cheung Law, Jiaxuan Tang, Wen Zhang, Ping Kwan Johnny Wong, Xiaojiang Yu, Feng Xu, Andrew T. S. Wee, Chim Seng Seet, and Wen Siang Lew*



Cite This: <https://doi.org/10.1021/acsnano.0c09404>



Read Online

ACCESS |



Metrics & More



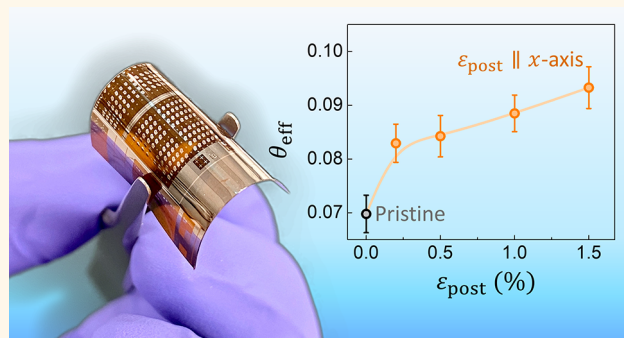
Article Recommendations



Supporting Information

ABSTRACT: Current-induced magnetization switching by spin–orbit torque generated in heavy metals offers an enticing realm for energy-efficient memory and logic devices. The spin Hall efficiency is a key parameter in describing the generation of spin current. Recent findings have reported enhancement of spin Hall efficiency by mechanical strain, but its origin remains elusive. Here, we demonstrate a 45% increase in spin Hall efficiency in the platinum/cobalt (Pt/Co) bilayer, of which 78% of the enhancement was preserved even after the strain was removed. Spin transparency and X-ray magnetic circular dichroism revealed that the enhancement was attributed to a bulk effect in the Pt layer. This was further confirmed by the linear relationship between the spin Hall efficiency and resistivity, which indicates an increase in skew-scattering. These findings shed light on the origin of enhancement and are promising in shaping future utilization of mechanical strain for energy-efficient devices.

KEYWORDS: spin Hall effect, spin–orbit torque, spin–orbit coupling, spin-torque ferromagnetic resonance, flexible substrate, mechanical strain



Since the demonstration of the spin Hall effect, the ability to manipulate magnetization with the use of current-induced spin–orbit torque (SOT) for energy-efficient memory and logic devices has attracted significant interest in the field of spintronics.^{1–6} The spin Hall effect capitalizes on the spin–orbit interaction in a nonmagnetic material to generate a pure spin current from an unpolarized charge current. In a heavy-metal/ferromagnetic layer (HM/FM) bilayer system, this results in a magnetic torque acting on the adjacent ferromagnet, thus allowing for SOT-induced magnetic switching.^{7–11} Heavy metals, such as platinum (Pt), tantalum (Ta), and tungsten (W), have been widely explored due to their strong spin–orbit interaction.^{3,12–16} In particular, Pt, in spite of its higher cost, has been pivotal and often seen as a benchmark in the development of spin Hall materials due to its large intrinsic spin Hall conductivity, easy growth, and ease of integration into existing manufacturing processes.

As such, attempts to improve the spin Hall efficiency, $\theta_{\text{eff}} = (2e/\hbar)T_{\text{int}}\sigma_{\text{SH}}\rho_{\text{Pt}}$, of Pt have been conducted extensively by understanding and manipulating the three distinct microscopic mechanisms: the skew, the side jump, and the intrinsic scattering.^{3,13,17–20} Here, e is the elementary charge, \hbar is the

reduced Planck's constant, T_{int} is the spin transparency, σ_{SH} is the spin Hall conductivity, and ρ_{Pt} is the electrical resistivity. To date, most of such attempts to enhance the spin Hall efficiency are focused on alloying the HM with lighter and more conductive metals,^{21–24} having insertion layers within the HM²⁵ and the varying deposition condition of the HM.^{26,27} Among the different methods used, a promising technique of enhancing the spin Hall efficiency is the use of mechanical strain. Recent work by T. Nan and E. Liu has shown that tensile strain enhances θ_{eff} in spin Hall materials, while compressive strain deteriorates it. However, the understanding behind the origin of the scattering mechanism that leads to this enhancement remains unclear, and more studies are needed to deepen our understanding of the physics of flexible spintronics devices.^{28,29}

Received: November 10, 2020

Accepted: May 6, 2021

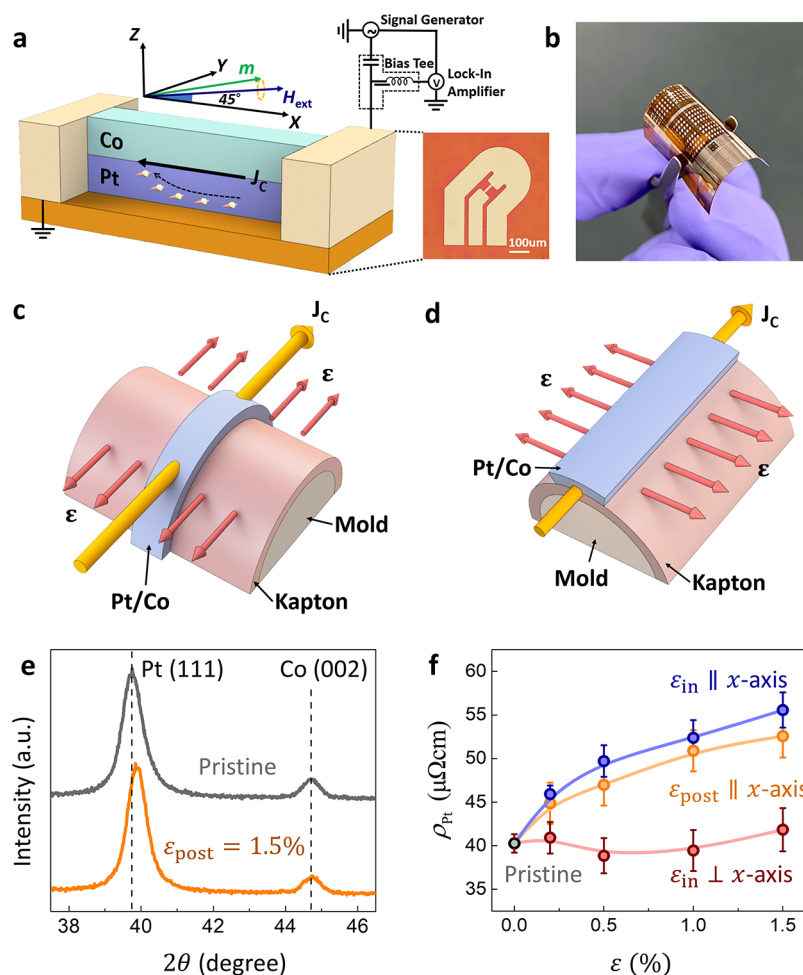


Figure 1. (a) Schematic illustration of a Pt/Co bilayer for the ST-FMR measurement. The green and navy arrows represent the precessing magnetization in the Co layer and applied external field, respectively. An RF current was applied along the longitudinal direction (x -axis) of the device, generating two orthogonal torques as it passes through the heavy metal. An optical image of the device is shown in the inset. (b) Photo of an array of strained ST-FMR devices on the flexible Kapton substrate. (c) Schematic of strain application onto the sample using a plastic mold in different directions. Strain in the parallel and (d) orthogonal direction as the radiofrequency current was applied during the ST-FMR measurement. (e) X-ray diffraction pattern of 25 nm thick Pt/Co samples showing the shift between the Pt(111) and the Cu(111) peak. The pristine sample is as-deposited, while the $\epsilon_{post} = 1.5\%$ sample was strained for 60 min before measurement. (f) Resistivity of Pt under tensile strain ϵ_{in} and when the substrate is relaxed after tensile strain ϵ_{post} is applied.

In this work, we study the effects of tensile strain on θ_{eff} in a Pt/Co bilayer system with the use of the spin-torque ferromagnetic resonance technique (ST-FMR) and demonstrate that the strain-induced θ_{eff} enhancement remains even after the strain has been removed. Spin transparency and X-ray absorption spectroscopy/X-ray magnetic circular dichroism (XAS/XMCD) results rule out the possibility of an improvement in the platinum/cobalt (Pt/Co) interface quality or interfacial spin-orbit interaction, thus leading us to hypothesize that the enhancement is a bulk effect in Pt. This is confirmed by the increased resistivity of Pt when strained, implying that tensile strain results in additional scattering within the Pt bulk. Furthermore, the switching current density is significantly reduced with the decrease in Gilbert damping parameter. These findings establish an understanding on how strain affects the spin Hall generation in a heavy metal and offer a very compelling justification to push the boundaries of existing spin Hall material for low-power SOT application.

RESULTS AND DISCUSSION

Material Characterization. The spin current generation mediated by the applied mechanical tensile strain on Pt was characterized using the ST-FMR measurement. Figure 1a depicts a schematic illustration of the measurement setup and device structure with an inset showing an optical image of the device. All films used in this study were prepared using magnetron sputtering onto unstrained Kapton at room temperature. As such, the initial internal stress from the fabrication of the films is the same for all samples and is thus negligible. The strain is applied after the device fabrication during the device characterization process. Bilayers Pt(5 nm)/Co(5 nm) were fabricated with a 5 nm titanium (Ti) seed and capping layer for film adhesion and oxidation prevention. A photo of an as-grown Pt/Co bilayer on the Kapton substrate is shown in Figure 1b, demonstrating its flexibility. Here, Pt plays the role of the heavy metal layer in producing SOTs *via* the spin Hall effect.

Figure 1c and d illustrates how the strain used in this study was applied after fabrication in two different configurations: tensile strain in the parallel and orthogonal direction to the radio-

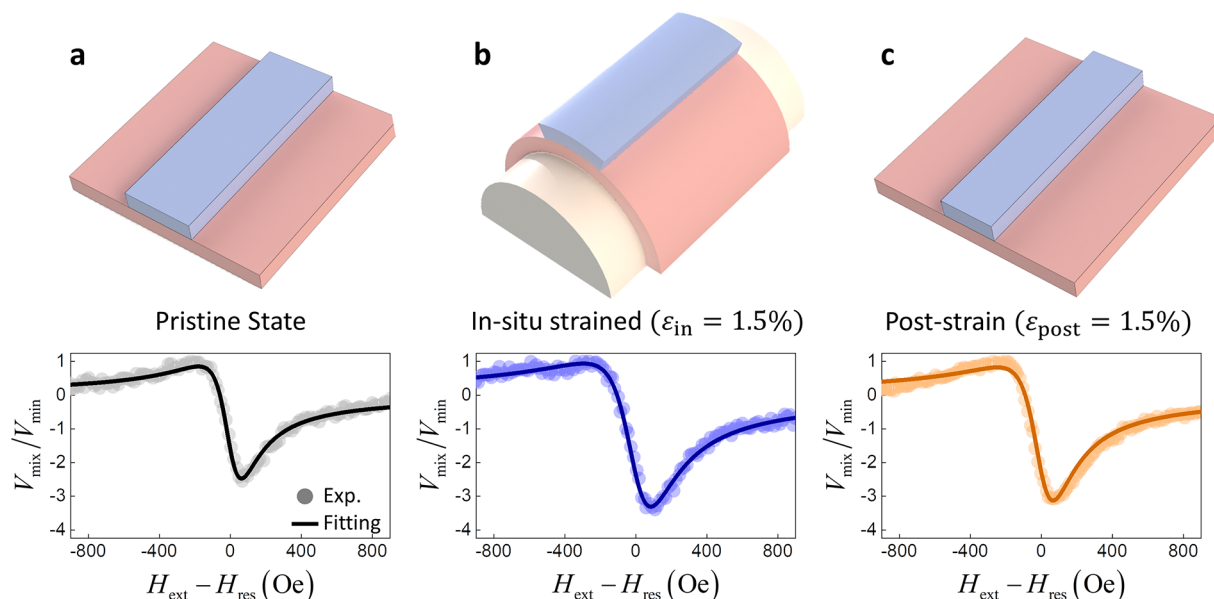


Figure 2. Schematic of sample and the measured ST-FMR spectra at 12 GHz at different strained conditions. The ST-FMR spectra V_{mix} are normalized to their minimum value. (a) Pristine, (b) while 1.5% strain is applied, and (c) after strain is removed with the sample flattened.

frequency (RF) current. The bending strain ε of the Kapton film in the bending direction was estimated by using $\varepsilon = t/2R$, where t and R are the total thickness of the substrate (120 μm) and bilayer structure and the curvature radius of the mold, respectively.³⁰ By varying the radius of curvature of the mold used, a tensile strain ε of 0 to approximately 1.5% was employed in this study. All strain used in this experiment is tensile strain if not specifically mentioned. *In situ* strain measurements are described by ε_{in} , while measurements taken after relaxing the strain are defined as $\varepsilon_{\text{post}}$, where $\varepsilon_{\text{post}}$ is the magnitude of the tensile strain applied for 60 min before relaxing it for measurement.

X-ray diffraction (XRD) was performed on two different Pt/Co thin-film samples. The first sample is kept in pristine condition, while the other was relaxed after applying a 1.5% tensile strain for 60 min. The XRD spectra are as presented in Figure 1e. After the application of strain, the Pt(111) peak makes a 0.14° shift to the left, while the Co(002) peak remains unchanged. This different behavior is due to the difference in Poisson's ratio between the two materials, with Pt having a larger ratio of 0.41 while Co is 0.29.³¹ The shift in Pt(111) peak suggests a change in Pt's bulk property and an increase in lattice constant due to the tensile strain. One such property change observed is the electrical resistivity (ρ_{Pt}) of Pt.

As tensile strain is applied along the longitudinal direction (x -axis) of the Pt microstrip, the strip expands and narrows along the direction of strain. Narrowing of the strip results in an increase in resistivity, which scales with the magnitude of the strain as shown in Figure 1f. This change can be described by the gauge factor given by $\text{GF} = (\Delta R/R)/\varepsilon$, where $\Delta R/R$ is the relative change in resistance and ε is the applied strain.³² For the Pt strained along the x -axis, the GF is calculated to be 10.5 ± 0.5 , which is consistent with previous findings.³³ Upon removing the strain, the film relaxes but the shift in lattice constant of Pt remains, indicating that the enhanced resistivity is still present due to internal stress. This residual strain is speculated to be the result of a change in lattice constant and the possibility of grain rotation mediated by grain boundary dislocation. The slight decrease in resistivity is caused by the relaxation of the substrate

reversing the narrowing of the strip. On the other hand, exerting strain in the transverse direction (y -axis) of the microstrip results in a less pronounced change in resistivity ρ_{Pt} .

Spin-Torque Generation Efficiency Analysis. To systematically evaluate the effects of tensile strain in the Pt layer on the spin-torque efficiency, ST-FMR was employed for bilayer Pt/Co. During the measurement, an RF current (J_{C}) was injected into the coplanar waveguide and flows along the long axis of the microstrip device (10 $\mu\text{m} \times 50 \mu\text{m}$). Simultaneously, an external magnetic field (H_{ext}) was applied at 45° . The longitudinal RF current passing through the Pt layer generates an oscillating transverse spin current by the spin Hall effect (SHE), which is then injected into the adjacent Co layer. The magnetization of Co experiences three different torques induced by the RF current: Oersted-field torque as current passes through the Co layer; field-like and damping-like torque produced by the current-induced SOT from the Pt layer. At the resonance field (H_{res}) when the microwave frequency matches the precessional frequency of the magnetization, the FMR condition is satisfied and the oscillating torques will result in the oscillation of the device resistance due to anisotropic magnetoresistance in the Co layer. The mixing of the RF current and oscillating resistance results in a rectified DC voltage signal (V_{mix}) across the device. Using a bias tee, V_{mix} can be measured during the microwave current application.

The ST-FMR spectra of bilayer Pt/Co was measured using a microwave power of 12 dBm and a frequency range between 8 and 17 GHz in steps of 1, and the measured V_{mix} is expressed as

$$V_{\text{mix}} = S \frac{(\Delta H/2)^2}{(H_{\text{ext}} - H_{\text{res}})^2 + (\Delta H/2)^2} + A \frac{(H_{\text{ext}} - H_{\text{res}})(\Delta H/2)}{(H_{\text{ext}} - H_{\text{res}})^2 + (\Delta H/2)^2} \quad (1)$$

where ΔH and H_{ext} are the spectra width and the applied external field and S and A are the magnitude of the symmetric and antisymmetric components of the V_{mix} , respectively. The symmetric Lorentzian contribution is produced when the spin Hall torque from the generated spin current and the magnet-

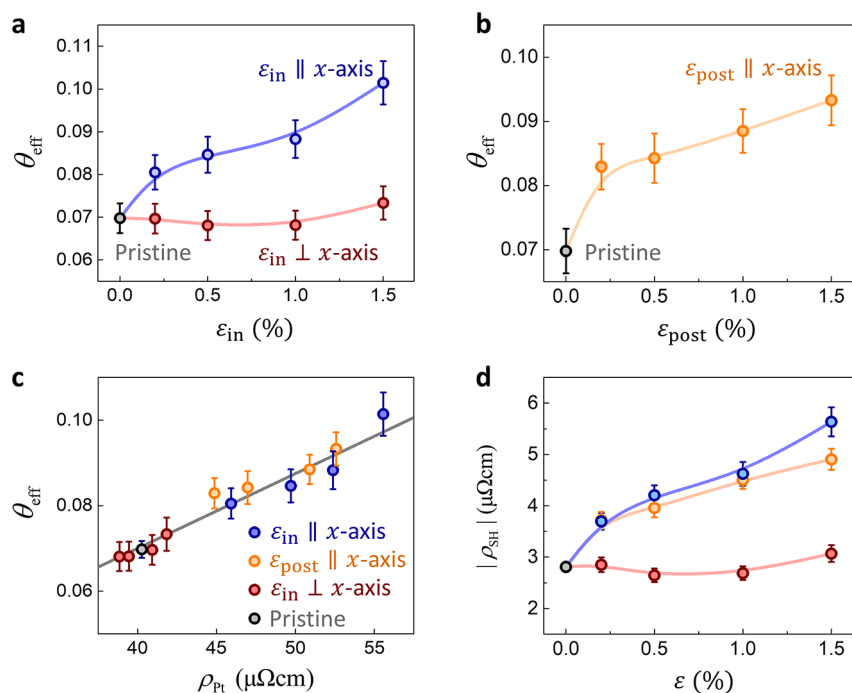


Figure 3. Spin Hall efficiency (a) as a function of *in situ* tensile strain ϵ_{in} and (b) after applying tensile strain ϵ_{post} for the Pt/Co bilayer. (c) Spin Hall efficiency dependence of the electrical resistivity of Pt. (d) Spin Hall resistivity of Pt dependence of tensile strain.

ization precession are in phase, while the antisymmetric Lorentzian contribution arises from the phase difference between the Oersted field and the field-like torque from the charge current passing through the Pt layer and the magnetization precession. The effective magnetization (M_{eff}) was obtained by an in-plane magnetization Kittel equation fitting $f = \gamma/2\pi\sqrt{(H_{\text{res}} + H_{\text{K}})(4\pi M_{\text{eff}} + H_{\text{res}} + H_{\text{K}})}$, where γ is the gyromagnetic ratio and H_{K} is the total magnetic anisotropy field. When exposed to tensile strain, M_{eff} decreases, and this corresponds to an enhancement in the H_{K} and surface anisotropy constant (K_{S}) given by $K_{\text{S}} = 2\pi M_{\text{S}}t_{\text{FM}}(M_{\text{S}} - M_{\text{eff}})$, where M_{S} and t_{FM} are the saturation magnetization of Co and thickness of the Co layer, respectively (refer to the Supporting Information (SI), Figures S1d and S2a).^{25,34,35} The M_{eff} decrease observed could also be attributed to the slight decrease in the M_{S} and increase in strain-induced anisotropy (refer to SI, Figure S3a).

The field-like torque in the Pt/Co bilayer is assumed to be negligible due to the sufficiently thick Pt layer used, and this assumption is consistent with previous work for Pt.^{16,36} With this, the spin Hall efficiency for the Pt/Co bilayer can be determined using the line-shape method described by the following equation:

$$\theta_{\text{eff}} = \frac{S}{A} \frac{e\mu_0 M_{\text{S}} t_{\text{FM}} t_{\text{NM}}}{\hbar} \sqrt{1 + \frac{4\pi M_{\text{eff}}}{H_{\text{res}}}} \quad (2)$$

where t_{NM} is the thickness of the Pt layer. The illustration in Figure 2 establishes the different stages of the experiment. For ease of comparison, all three ST-FMR spectra of bilayer Pt/Co were normalized to its minimum value. From the line-shape equation, the magnitude of S/A is proportional to the spin Hall efficiency, which implies that a larger $V_{\text{mix}}/V_{\text{min}}$ magnitude corresponds to a larger spin Hall efficiency.

Using the $V_{\text{mix}}/V_{\text{min}}$ value for the pristine Pt/Co as a benchmark in Figure 2a, the effects of strain on the spin Hall

efficiency can be observed. At $\epsilon_{\text{in}} = 1.5\%$, $V_{\text{mix}}/V_{\text{min}}$ increases by 36% as shown Figure 2b, suggesting that an enhancement in the spin Hall efficiency was brought about by the strain, which was previously reported.^{28,29,37} However, a more striking observation was made after the removal of the strain in Figure 2c, which shows that the strain-induced increment was retained. The corresponding spin Hall efficiency was calculated and is summarized in Figure 3a and b.

The θ_{eff} dependence of tensile strain in the parallel and orthogonal direction to the current is shown in Figure 3a. Here, θ_{eff} increases proportionally with tensile strain along the direction of current. When $\epsilon_{\text{in}} = 1.5\%$ is applied, θ_{eff} is enhanced by 45% from 0.070 ± 0.003 to 0.101 ± 0.005 . Interestingly, upon removing the tensile strain in this direction, 78% of the θ_{eff} enhancement is retained, giving a value of 0.093 ± 0.007 even when the substrate is flattened and relaxed as shown in Figure 3b. However, not all tensile strain will result in an enhancement. For the tensile strain to enhance the θ_{eff} , the direction at which the strain is applied is crucial. Applying strain in the orthogonal direction did not affect the θ_{eff} , which is consistent with previous work.²⁸ Based on $\theta_{\text{eff}} = T_{\text{int}}\theta_{\text{SH}}$, where θ_{SH} is the spin Hall angle of Pt, the origin of the θ_{eff} enhancement can be categorized into either (i) an interfacial or (ii) bulk effect. To better comprehend the physics and distinguish between the two effects of strain on the Pt/Co interface, spin transparency and XMCD were measured. FMR measurements were performed on a Pt/Co bilayer thin film, and the ϵ_{post} strain was applied before measurement. Plotting θ_{eff} as a function of ρ_{Pt} , a linear relation is observed in Figure 3c. Both θ_{eff} and ρ_{Pt} increase by about 40% when $\epsilon_{\text{in}} = 1.5\%$ is applied. However, the increase in θ_{eff} is lower than previous work reporting that the increase in resistivity will result in a much greater increase in spin Hall angle.²⁶ Varying pressure during film deposition affects the growth condition of the HM layer directly as compared to the use of mechanical strain. Hence, it is difficult to compare the two methods directly, as their effects on the HM layer to change the resistivity are

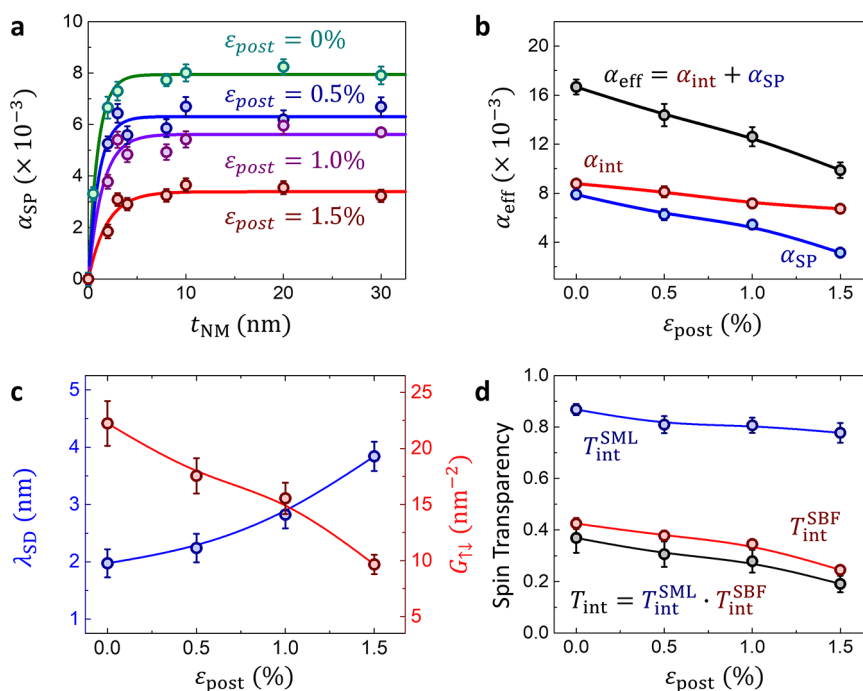


Figure 4. (a) Damping parameter due to spin pumping of the Pt/Co bilayer with varying Pt thickness for samples after ϵ_{post} application. (b) α_{eff} (c) λ_{SD} and $G^{\uparrow\downarrow}$, and (d) spin transparency T_{int} as a function of ϵ_{post} application.

different. From Figure 3d, the spin Hall resistivity, $\rho_{\text{SH}} = \theta_{\text{eff}} \rho_{\text{Pt}}$ increases in a similar trend to θ_{eff} when strain is applied.

Gilbert Damping and Spin Transparency Analysis. The effective Gilbert damping (α_{eff}) was calculated from the line width of the FMR measurement of the Pt/Co bilayer, which can be expressed as $\Delta H = \Delta H_0 + 4\pi\alpha_{\text{eff}}/\gamma$, where ΔH_0 is the inhomogeneous broadening term originating from sample imperfections, which are assumed to be frequency independent. Two-magnon scattering is not observed in the data due to the linear dependence of the FMR line width with frequency (refer to SI, Figure S4).³⁸ The magnetic proximity effect is assumed to be negligible as the M_{S} of Co falls within range of pure Co bulk (refer to SI, Figure S3b).^{34,39–43} The α_{eff} of the Pt/Co bilayer is mainly contributed by the intrinsic Gilbert damping (α_{int}) from Co and the damping introduced by spin pumping effect (α_{SP}) due to the adjacent Pt.^{44,45} A Pt thickness dependence of spin pumping induced damping was performed as shown in Figure 4a, and their relation can be described by

$$\alpha_{\text{eff}} = \alpha_{\text{int}} + \frac{g\mu_{\text{B}}}{4\pi M_{\text{S}}(t_{\text{FM}} - t_{\text{d}})} G^{\uparrow\downarrow} (1 - e^{-2t_{\text{NM}}/\lambda_{\text{SD}}}) \quad (3)$$

where g is the g -factor, t_{d} is the magnetic dead layer thickness, $G^{\uparrow\downarrow}$ is the effective spin-mixing conductance due to Pt, and λ_{SD} is the spin diffusion length. Using the obtained α_{SP} , the two main Gilbert damping contributions are consolidated and compared in Figure 4b. The change in intrinsic damping from the Co is negligibly small as compared to the decrease in α_{SP} . This outcome matches our XRD result that the Co lattice constant is not affected by ϵ_{post} . Pt on the other hand is greatly affected by the tensile strain, and since α_{SP} is heavily dependent on the interface between Pt and Co, any deterioration of the interface will translate to a decrease in α_{SP} . The effective damping drops by 40% from $(1.7 \pm 0.1) \times 10^{-3}$ to $(0.99 \pm 0.06) \times 10^{-3}$ primarily attributed to the decrease in α_{SP} .

From Figure 4c, the ϵ_{post} dependence of the spin diffusion length and spin-mixing conductance of the Pt/Co bilayer is

shown. The spin diffusion length increases inversely with the spin-mixing conductance when strain is introduced. Based on the Elliott–Yafet (EY) mechanism, an increased Pt electrical resistivity should lead to shorter spin diffusion length; however the opposite is observed. This indicates a possible decrease in interfacial spin–orbit coupling (ISOC), which was reflected from the XMCD analysis later.⁴⁶

The interfacial intrinsic spin transparency T_{int} between an FM/HM is more often than not below unity due to two main contributing phenomena known as spin memory loss (SML) and spin backflow (SBF). SML is the interfacial spin–orbit scattering that results in a loss in spin transmission. For a Pt/Co interface with in-plane magnetic anisotropy, the effects of SML on T_{int} can be approximated using $T_{\text{int}}^{\text{SML}} \approx 1 - 0.23K_{\text{S}}$.^{25,27,47} SBF on the other hand is attributed to the finite spin-mixing conductance at the interface and can be analyzed using the drift-diffusion model given by

$$T_{\text{int}}^{\text{SBF}} = \frac{G^{\uparrow\downarrow} \tanh(t_{\text{NM}}/2\lambda_{\text{SD}})}{G^{\uparrow\downarrow} \coth(t_{\text{NM}}/2\lambda_{\text{SD}}) + (\sigma/\lambda_{\text{SD}})(h/2e^2)} \quad (4)$$

where $T_{\text{int}}^{\text{SBF}}$ is the spin transparency and σ is the electrical conductivity of Pt.^{25,27,48,49} Figure 4d shows the effects of tensile strain on the $T_{\text{int}}^{\text{SML}}$ and $T_{\text{int}}^{\text{SBF}}$ along with the T_{int} , which can be obtained by taking the product of the two contributing factors. At $\epsilon_{\text{post}} = 1.5\%$, the T_{int} decreases by 48% from 0.37 ± 0.06 to 0.19 ± 0.03 with the majority of the effect coming from the $T_{\text{int}}^{\text{SBF}}$. The greater decline in $T_{\text{int}}^{\text{SBF}}$ as compared to $T_{\text{int}}^{\text{SML}}$ is hypothesized to be attributed to the change in interfacial spin–orbit interaction at the Pt/Co interface. This decrease in T_{int} suggests that the enhancement in θ_{eff} is not a result of an improvement of the interfacial quality.

XAS/XMCD Measurement. To further verify that the θ_{eff} enhancement is not attributed to the interface between the Pt/Co bilayer, XAS/XMCD measurements were performed. The total electron yield intensities μ_{+} and μ_{-} around the L_2 and L_3

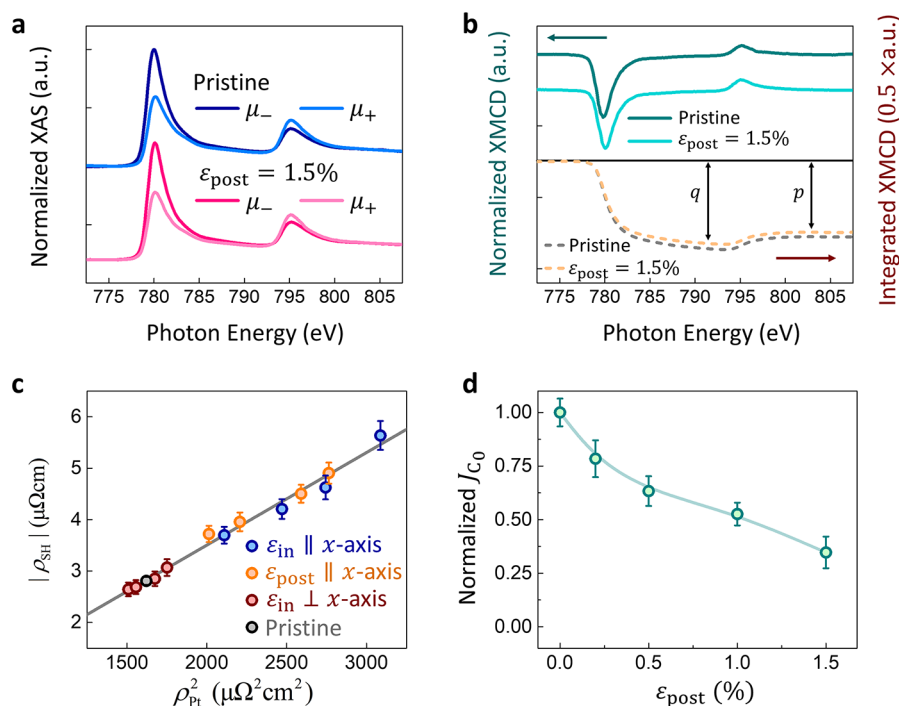


Figure 5. (a) Normalized XAS at the Co $L_{2,3}$ absorption edge. (b) Corresponding normalized XMCD spectra with their integrated intensities. The vertical arrows indicate the values of p and q , derived from the integrals of the dichroic signals. (c) Spin Hall resistivity as a function of the squared Pt resistivity. (d) Normalized switching current density as a function of ϵ_{post} application.

edges for Co (770–810 eV) were measured at the grazing incidence, as shown in Figure 5a and b. By applying the sum rules to the XMCD spectra, the orbital to spin magnetic moment ratio (m_L/m_S) can be obtained as follows:

$$\frac{m_L}{m_S} = \frac{2q}{9p - 6q} \quad (5)$$

where p is the integral of the dichroic signal of the L_3 peak alone and q is the integrated dichroism over both the L_2 and L_3 edges.^{26,50,51} The m_L/m_S ratio of Co decreases by 22% from 0.394 ± 0.03 to 0.304 ± 0.02 when the strain was applied, implying a reduction in spin–orbit coupling.^{52,53} This suggests that the enhancement in θ_{eff} revealed by our spin transparency measurement, is not caused by an enhanced ISOC, while the bulk effect may prevail. The decreasing trend of Co m_L/m_S ratio upon the strain application seems to be in line with the inverse proportional relationship between λ_{SD} and ISOC.⁴⁶

To date, it has been reported that the intrinsic scattering mechanism dominates over the extrinsic in 4d and 5d transition metals such as Pd, Pt, Ta, and W.^{3,13} In a nonalloyed metal such as Pt, the side jump scattering contribution can be assumed to be negligibly small as compared to the skew-scattering.⁵⁴ Therefore, the only extrinsic contribution considered in the Pt/Co system is the skew-scattering. By assuming the total spin Hall conductivity of the system to be the sum of the intrinsic and extrinsic contribution, the spin Hall resistivity can be expressed by the following equation:

$$-\rho_{\text{SH}} = \sigma_{\text{SH}}^{\text{int}} \rho_{\text{Pt}}^2 - \rho_{\text{SH}}^{\text{SS}} \quad (6)$$

where $\sigma_{\text{SH}}^{\text{int}}$ is the intrinsic spin Hall conductivity of Pt and $\rho_{\text{SH}}^{\text{SS}}$ is the spin Hall resistivity influenced by the skew-scattering mechanism.^{55,56} By plotting the $|\rho_{\text{SH}}|$ as a function of the ρ_{Pt}^2 in Figure 5c, $\sigma_{\text{SH}}^{\text{int}}$ is found to be $(1.79 \pm 0.05) \times 10^5 (\hbar/2e) \Omega\text{m}$, which is consistent with previous reports of a value of $1.6 \times$

$10^5 (\hbar/2e) \Omega\text{m}$.^{57,58} Since there is little change to the intrinsic contribution of Pt, this implies that the source of the enhancement is contributed by extrinsic scattering. From the linear relation, $\sigma_{\text{SH}}^{\text{SS}}$ is calculated to be $(1.09 \pm 0.06) \times 10^5 (\hbar/2e) \Omega\text{m}$. Additional skew-scattering as a result of the tensile strain makes up for 38% of the total spin Hall conductivity, and this is larger than previous works reporting only 28% contribution by varying the deposition condition of Pt.^{54,57} Due to the nature of nonalloyed metals, the contribution from the intrinsic scattering in Pt dominates. However, the extrinsic contribution from the skew-scattering grows when tensile strain is introduced, resulting in enhanced θ_{eff} . Apart from the θ_{eff} enhancement, another benefit of the use of tensile strain is the reduction in the switching current density J_{C0} required for an SOT device. J_{C0} can be estimated using the following equation:

$$J_{\text{C0}} \approx \frac{2e}{\hbar} \frac{\alpha_{\text{eff}}}{\theta_{\text{eff}}} \left(\frac{4\pi M_{\text{eff}}}{2} \right) M_{\text{S}} t_{\text{FM}} \quad (7)$$

Since J_{C0} is proportional to the ratio between α_{eff} and θ_{eff} , a decrease in the ratio implies a lower J_{C0} , as shown in Figure 5d. At $\epsilon_{\text{post}} = 1.5\%$, J_{C0} decreases by 65%, making tensile strain a very viable and flexible method of achieving low-power-consumption SOT devices.

CONCLUSIONS

In summary, we have demonstrated the use of tensile strain to enhance θ_{eff} and showed that 78% of the enhancement can be retained even after removing the strain. The result from spin transparency and XMCD measurements suggests that the enhancement is of bulk origin. With strain treatment, the spin Hall angle, $\theta_{\text{SH}} = \theta_{\text{eff}}/T_{\text{inv}}$ of Pt could potentially be much greater than the previously reported value of ~ 0.30 after accounting for

the spin transparency at $\epsilon_{\text{post}} = 1.5\%$.⁵⁹ Moreover, the J_{CO} required is drastically reduced due to the decrease in the $\alpha_{\text{eff}}/\theta_{\text{eff}}$ ratio. Our findings will aid in the development of power-efficient and flexible spintronics devices through mechanical strain engineering. Directional control of strain during application plays a critical role in the device functionality, and one potential approach includes the use of a microelectromechanical system (MEMS) and origami architected microbots, which can guide strain in a specific direction.

METHODS

Sample Growth and Preparation. All samples were sputter-deposited onto an unstrained Kapton substrate at room temperature using an Ar pressure of 2 mTorr and a base pressure lower than 5×10^{-8} Torr. Two-inch-diameter targets with a purity of 99.99% were used. The stacked structure used for this study is flexible Kapton substrate/Ti (5 nm)/Pt(t_{NM} nm)/Co(5 nm)/Ti (5 nm) with t_{NM} fixed at 5 nm for the spin Hall efficiency measurements. Five nanometers of Ti was introduced at the top and bottom to improve adhesion and prevent oxidation of the stacked structure. Resistivities of Pt microstrips were determined using a semiconductor analyzer, and the microstrips used were fabricated using optical lithography. The ST-FMR devices were then patterned into $10 \mu\text{m} \times 50 \mu\text{m}$ rectangular microstrips using an optical lithography technique; thereafter a coplanar waveguide (CPW) structure was fabricated onto the strips. Plastic molds of predetermined curvature for the application of tensile strain were 3D printed using a polylactic acid filament.

Characterization and Electrical Measurement. For *in situ* strain (ϵ_{in}) samples were strained during the measurement, while strain-treated (ϵ_{post}) samples were strained for 60 min before their respective measurements. The magnetization of the Co layer and the crystallinity of the stack were measured using a vibrating sample magnetometer and X-ray diffraction technique. RF current was generated from the Keysight N5183B analog signal generator and injected into the CPW electrode. The microwave power was fixed at 12 dBm, and the measured frequencies were varied between 8 and 17 GHz with an increment step size of 1 GHz. The θ_{eff} values are averaged across five devices. An in-plane external magnetic field (H_{ext}) is swept while injecting RF current at 45° relative to one another. The rectified DC voltage is then passed through a bias tee and into a Zurich Instruments lock-in amplifier for detection. The Gilbert damping was used to obtain the spin pumping contribution, and spin transparency was measured using FMR.

X-ray Magnetic Circular Dichroism Measurement. XMCD measurements were performed at the Co $L_{2,3}$ edge using circularly polarized X-rays at the Surface, Interface and Nanostructure Science (SINS) beamline of the Singapore Synchrotron Light Source.^{60,61} All spectra were measured at room temperature in the total-electron-yield mode with a fixed helicity of 80% circularly polarized X-rays and opposite magnetic fields up to ± 1 T. The angle of incidence of the photon beam was positioned at 60° with respect to the sample surface normal. The orbital to spin magnetic moment ratio was extracted using the sum rules.

ASSOCIATED CONTENT

Supporting Information

The Supporting Information is available free of charge at <https://pubs.acs.org/doi/10.1021/acsnano.0c09404>.

Additional discussion on the ST-FMR spectra and line width, strain dependence of in-plane uniaxial magnetic anisotropy field and magnetization saturation in Co, and the negligible SOT contribution from the field-like torque in the Pt layer and Ti layer (PDF)

AUTHOR INFORMATION

Corresponding Author

Wen Siang Lew – School of Physical & Mathematical Sciences, Nanyang Technological University, Singapore 637371; orcid.org/0000-0002-5161-741X; Email: wensiang@ntu.edu.sg

Authors

Grayson Dao Hwee Wong – School of Physical & Mathematical Sciences, Nanyang Technological University, Singapore 637371; GLOBALFOUNDRIES Singapore Pte. Ltd., Singapore 738406; orcid.org/0000-0003-1661-2346

Zhan Xu – School of Physical & Mathematical Sciences, Nanyang Technological University, Singapore 637371; MIIT Key Laboratory of Advanced Metallic and Intermetallic Materials Technology, School of Materials Science and Engineering, Nanjing University of Science and Technology, Nanjing 210094, China

Weiliang Gan – School of Physical & Mathematical Sciences, Nanyang Technological University, Singapore 637371

Calvin Ching Ian Ang – School of Physical & Mathematical Sciences, Nanyang Technological University, Singapore 637371

Wai Cheung Law – School of Physical & Mathematical Sciences, Nanyang Technological University, Singapore 637371; GLOBALFOUNDRIES Singapore Pte. Ltd., Singapore 738406

Jiaxuan Tang – MIIT Key Laboratory of Advanced Metallic and Intermetallic Materials Technology, School of Materials Science and Engineering, Nanjing University of Science and Technology, Nanjing 210094, China

Wen Zhang – School of Microelectronics, Northwestern Polytechnical University, Xi'an 710072, China

Ping Kwan Johnny Wong – School of Microelectronics, Northwestern Polytechnical University, Xi'an 710072, China; orcid.org/0000-0003-4645-0384

Xiaojiang Yu – Singapore Synchrotron Light Source, National University of Singapore, Singapore 117603

Feng Xu – MIIT Key Laboratory of Advanced Metallic and Intermetallic Materials Technology, School of Materials Science and Engineering, Nanjing University of Science and Technology, Nanjing 210094, China; orcid.org/0000-0001-5802-7925

Andrew T. S. Wee – Department of Physics and Centre for Advanced 2D Materials and Graphene Research Centre, National University of Singapore, Singapore 117546; orcid.org/0000-0002-5828-4312

Chim Seng Seet – GLOBALFOUNDRIES Singapore Pte. Ltd., Singapore 738406

Complete contact information is available at: <https://pubs.acs.org/doi/10.1021/acsnano.0c09404>

Author Contributions

G.D.H.W. conceived the idea, designed this work, and drafted the manuscript. G.D.H.W. and Z.X. fabricated the devices and collected the data. W.C.L. assisted in the development of the experimental setup. W.L.G., C.C.I.A., and Z.X. made scientific comments on the results. J.T. and X.Y. performed the XRD and XAS measurements. W.Z. and P.K.J.W. analyzed the XAS/XMCD data. W.S.L., C.S.S., A.T.S.W., and F.X. coordinated and supervised the entire work. All authors contributed to the discussions and the revision of the final manuscript.

Notes

The authors declare no competing financial interest.

ACKNOWLEDGMENTS

This work is supported by an Industry-IHL Partnership Program (NRF2015-IIP001-001) and an EDB-IPP (RCA – 17/284) grant. This work is also supported by the RIE2020 ASTAR AME IAF-ICP grant (No. I1801E0030). W.Z. and P.K.J.W. acknowledge financial support by the Fundamental Research Funds for the Central Universities. The authors would like to acknowledge the Singapore Synchrotron Light Source (SSLS) for providing the facility necessary for conducting the research. The Laboratory is a National Research Infrastructure under the National Research Foundation Singapore.

REFERENCES

- (1) Kato, Y. K.; Myers, R. C.; Gossard, A. C.; Awschalom, D. D. Observation of the Spin Hall Effect in Semiconductors. *Science* **2004**, *306*, 1910–1913.
- (2) Wunderlich, J.; Kaestner, B.; Sinova, J.; Jungwirth, T. Experimental Observation of the Spin-Hall Effect in a Two-Dimensional Spin-Orbit Coupled Semiconductor System. *Phys. Rev. Lett.* **2005**, *94*, 047204.
- (3) Tanaka, T.; Kontani, H.; Naito, M.; Naito, T.; Hirashima, D. S.; Yamada, K.; Inoue, J. Intrinsic Spin Hall Effect and Orbital Hall Effect in 4D And 5D Transition Metals. *Phys. Rev. B: Condens. Matter Mater. Phys.* **2008**, *77*, 165117.
- (4) Guo, G.-Y.; Murakami, S.; Chen, T.-W.; Nagaosa, N. Intrinsic Spin Hall Effect in Platinum: First-Principles Calculations. *Phys. Rev. Lett.* **2008**, *100*, 096401.
- (5) Saitoh, E.; Ueda, M.; Miyajima, H.; Tatara, G. Conversion of Spin Current into Charge Current at Room Temperature: Inverse Spin-Hall Effect. *Appl. Phys. Lett.* **2006**, *88*, 182509.
- (6) Kimura, T.; Otani, Y.; Sato, T.; Takahashi, S.; Maekawa, S. Room-Temperature Reversible Spin Hall Effect. *Phys. Rev. Lett.* **2007**, *98*, 156601.
- (7) Emori, S.; Bauer, U.; Ahn, S.-M.; Martinez, E.; Beach, G. S. Current-Driven Dynamics of Chiral Ferromagnetic Domain Walls. *Nat. Mater.* **2013**, *12*, 611–616.
- (8) Xu, Z.; Wong, G. D. H.; Tang, J.; Liu, E.; Gan, W.; Xu, F.; Lew, W. S. Giant Spin Hall Effect in Cu-Tb Alloy Thin Films. *ACS Appl. Mater. Interfaces* **2020**, *12*, 32898–32904.
- (9) Valenzuela, S.; Tinkham, M. Electrical Detection of Spin Currents: The Spin-Current Induced Hall Effect. *J. Appl. Phys.* **2007**, *101*, 09B103.
- (10) Hirsch, J. Spin Hall Effect. *Phys. Rev. Lett.* **1999**, *83*, 1834.
- (11) Zhang, S. Spin Hall Effect in the Presence of Spin Diffusion. *Phys. Rev. Lett.* **2000**, *85*, 393.
- (12) Tao, X.; Liu, Q.; Miao, B.; Yu, R.; Feng, Z.; Sun, L.; You, B.; Du, J.; Chen, K.; Zhang, S. Self-Consistent Determination of Spin Hall Angle and Spin Diffusion Length in Pt and Pd: The Role of the Interface Spin Loss. *Sci. Adv.* **2018**, *4*, No. eaat1670.
- (13) Morota, M.; Niimi, Y.; Ohnishi, K.; Wei, D.; Tanaka, T.; Kontani, H.; Kimura, T.; Otani, Y. Indication of Intrinsic Spin Hall Effect in 4D and 5D Transition Metals. *Phys. Rev. B: Condens. Matter Mater. Phys.* **2011**, *83*, 174405.
- (14) Pai, C.-F.; Liu, L.; Li, Y.; Tseng, H.; Ralph, D.; Buhrman, R. Spin Transfer Torque Devices Utilizing the Giant Spin Hall Effect of Tungsten. *Appl. Phys. Lett.* **2012**, *101*, 122404.
- (15) Liu, L.; Pai, C.-F.; Li, Y.; Tseng, H.; Ralph, D.; Buhrman, R. Spin-Torque Switching with the Giant Spin Hall Effect of Tantalum. *Science* **2012**, *336*, 555–558.
- (16) Liu, L.; Moriyama, T.; Ralph, D.; Buhrman, R. Spin-Torque Ferromagnetic Resonance Induced by the Spin Hall Effect. *Phys. Rev. Lett.* **2011**, *106* (3), 036601.
- (17) Smit, J. The Spontaneous Hall Effect in Ferromagnetics II. *Physica* **1958**, *24*, 39–51.
- (18) Berger, L. Side-Jump Mechanism for the Hall Effect of Ferromagnets. *Phys. Rev. B* **1970**, *2*, 4559.
- (19) Karplus, R.; Luttinger, J. Hall Effect in Ferromagnetics. *Phys. Rev.* **1954**, *95*, 1154.
- (20) Sinova, J.; Culcer, D.; Niu, Q.; Sinitsyn, N.; Jungwirth, T.; MacDonald, A. H. Universal Intrinsic Spin Hall Effect. *Phys. Rev. Lett.* **2004**, *92*, 126603.
- (21) Ramaswamy, R.; Wang, Y.; Elyasi, M.; Motapothula, M.; Venkatesan, T.; Qiu, X.; Yang, H. Extrinsic Spin Hall Effect in $\text{Cu}_{1-x}\text{Pt}_x$. *Phys. Rev. Appl.* **2017**, *8*, 024034.
- (22) Wong, G.; Law, W.; Tan, F.; Gan, W.; Ang, C.; Xu, Z.; Seet, C.; Lew, W. Thermal Behavior of Spin-Current Generation in $\text{Pt}_x\text{Cu}_{1-x}$ Devices Characterized through Spin-Torque Ferromagnetic Resonance. *Sci. Rep.* **2020**, *10*, 1–8.
- (23) Zhu, L.; Ralph, D. C.; Buhrman, R. A. Enhancement of Spin Transparency by Interfacial Alloying. *Phys. Rev. B: Condens. Matter Mater. Phys.* **2019**, *99*, 180404.
- (24) Fert, A.; Levy, P. M. Spin Hall Effect Induced by Resonant Scattering on Impurities in Metals. *Phys. Rev. Lett.* **2011**, *106*, 157208.
- (25) Zhu, L.; Buhrman, R. Maximizing Spin-Orbit-Torque Efficiency of Pt/Ti Multilayers: Trade-Off between Intrinsic Spin Hall Conductivity and Carrier Lifetime. *Phys. Rev. Appl.* **2019**, *12*, 051002.
- (26) Lee, J. W.; Oh, Y.-W.; Park, S.-Y.; Figueroa, A. I.; Van Der Laan, G.; Go, G.; Lee, K.-J.; Park, B.-G. Enhanced Spin-Orbit Torque by Engineering Pt Resistivity in Pt/Co/AlO_x Structures. *Phys. Rev. B: Condens. Matter Mater. Phys.* **2017**, *96*, 064405.
- (27) Nguyen, M.-H.; Ralph, D.; Buhrman, R. Spin Torque Study of the Spin Hall Conductivity and Spin Diffusion Length in Platinum Thin Films with Varying Resistivity. *Phys. Rev. Lett.* **2016**, *116*, 126601.
- (28) Liu, E.; Fache, T.; Cespedes-Bercoff, D.; Zhang, Z.; Petit-Watelot, S.; Mangin, S.; Xu, F.; Rojas-Sánchez, J.-C. Strain-Enhanced Charge-to-Spin Conversion in Ta/Fe/Pt Multilayers Grown on Flexible Mica Substrate. *Phys. Rev. Appl.* **2019**, *12*, 044074.
- (29) Filianina, M.; Hanke, J.-P.; Lee, K.; Han, D.-S.; Jaiswal, S.; Rajan, A.; Jakob, G.; Mokrousov, Y.; Kläui, M. Electric-Field Control Of Spin-Orbit Torques in Perpendicularly Magnetized W/CoFeB/MgO Films. *Phys. Rev. Lett.* **2020**, *124*, 217701.
- (30) Zhang, Z.; Liu, E.; Zhang, W.; Wong, P. K. J.; Xu, Z.; Hu, F.; Li, X.; Tang, J.; Wee, A. T. S.; Xu, F. Mechanical Strain Manipulation of Exchange Bias Field and Spin Dynamics in FeCo/IrMn Multilayers Grown on Flexible Substrates. *ACS Appl. Mater. Interfaces* **2019**, *11*, 8258–8265.
- (31) De Jong, M.; Chen, W.; Angsten, T.; Jain, A.; Notestine, R.; Gamst, A.; Sluiter, M.; Ande, C. K.; Van Der Zwaag, S.; Plata, J. J. Charting the Complete Elastic Properties of Inorganic Crystalline Compounds. *Sci. Data* **2015**, *2*, 1–13.
- (32) Zhang, Y.-Z.; Lee, K. H.; Anjum, D. H.; Sougrat, R.; Jiang, Q.; Kim, H.; Alshareef, H. N. MXenes Stretch Hydrogel Sensor Performance to New Limits. *Sci. Adv.* **2018**, *4*, No. eaat0098.
- (33) Fricke, S.; Friedberger, A.; Mueller, G.; Seidel, H.; Schmid, U. In, Strain Gauge Factor and TCR of Sputter Deposited Pt Thin Films Up to 850°C. *IEEE Sensor Conference* **2008**, *2008*, 1532–1535.
- (34) Bouloussa, H.; Ramaswamy, R.; Roussigné, Y.; Stashkevich, A.; Yang, H.; Belmeguenai, M.; Chérif, S. Pt Concentration Dependence of the Interfacial Dzyaloshinskii–Moriya Interaction, the Gilbert Damping Parameter and the Magnetic Anisotropy in Py/Cu_{1-x}Pt_x Systems. *J. Phys. D: Appl. Phys.* **2019**, *52*, 055001.
- (35) Nguyen, M.-H.; Zhao, M.; Ralph, D.; Buhrman, R. Enhanced Spin Hall Torque Efficiency in Pt_{100-x}Al_x and Pt_{100-x}Hf_x Alloys Arising from the Intrinsic Spin Hall Effect. *Appl. Phys. Lett.* **2016**, *108*, 242407.
- (36) Skowroński, W.; Karwacki, Ł.; Ziętek, S.; Kanak, J.; Łazarski, S.; Grochot, K.; Stobiecki, T.; Kuświk, P.; Stobiecki, F.; Barnaś, J. Determination of Spin Hall Angle in Heavy-Metal/Co–Fe–B-Based Heterostructures with Interfacial Spin-Orbit Fields. *Phys. Rev. Appl.* **2019**, *11*, 024039.
- (37) Nan, T.; Hu, J. M.; Dai, M.; Emori, S.; Wang, X.; Hu, Z.; Matyushov, A.; Chen, L. Q.; Sun, N. A Strain-Mediated Magnetoelectric-Spin-Torque Hybrid Structure. *Adv. Funct. Mater.* **2019**, *29*, 1806371.

- (38) Arias, R.; Mills, D. Extrinsic Contributions to the Ferromagnetic Resonance Response of Ultrathin Films. *Phys. Rev. B: Condens. Matter Mater. Phys.* **1999**, *60*, 7395.
- (39) Geissler, J.; Goering, E.; Justen, M.; Weigand, F.; Schütz, G.; Langer, J.; Schmitz, D.; Maletta, H.; Mattheis, R. Pt Magnetization Profile in a Pt/Co Bilayer Studied by Resonant Magnetic X-Ray Reflectometry. *Phys. Rev. B: Condens. Matter Mater. Phys.* **2001**, *65*, 020405.
- (40) Koyama, T.; Guan, Y.; Hibino, Y.; Suzuki, M.; Chiba, D. Magnetization Switching by Spin-Orbit Torque in Pt with Proximity-Induced Magnetic Moment. *J. Appl. Phys.* **2017**, *121*, 123903.
- (41) Ferrer, S.; Alvarez, J.; Lundgren, E.; Torrelles, X.; Fajardo, P.; Boscherini, F. Surface X-Ray Diffraction from Co/Pt(111) Ultrathin Films and Alloys: Structure and Magnetism. *Phys. Rev. B: Condens. Matter Mater. Phys.* **1997**, *56*, 9848.
- (42) White, T.; Bailey, T.; Pierce, M.; Miller, C. W. Strong Spin Pumping in Permalloy-Iridium Heterostructures. *IEEE Magn. Lett.* **2017**, *8*, 1–4.
- (43) Zhu, L.; Ralph, D.; Buhrman, R. Irrelevance of Magnetic Proximity Effect to Spin-Orbit Torques in Heavy-Metal/Ferromagnet Bilayers. *Phys. Rev. B: Condens. Matter Mater. Phys.* **2018**, *98*, 134406.
- (44) Mosendz, O.; Vlaminck, V.; Pearson, J.; Fradin, F.; Bauer, G.; Bader, S.; Hoffmann, A. Detection and Quantification of Inverse Spin Hall Effect from Spin Pumping in Permalloy/Normal Metal Bilayers. *Phys. Rev. B: Condens. Matter Mater. Phys.* **2010**, *82*, 214403.
- (45) Shaw, J. M.; Nembach, H. T.; Silva, T. J. Determination of Spin Pumping as a Source of Linewidth in Sputtered Co₉₀Fe₁₀/Pd Multilayers by Use of Broadband Ferromagnetic Resonance Spectroscopy. *Phys. Rev. B: Condens. Matter Mater. Phys.* **2012**, *85*, 054412.
- (46) Ma, L.; Lang, L.; Kim, J.; Yuan, Z.; Wu, R.; Zhou, S.; Qiu, X. Spin Diffusion Length and Spin Hall Angle in Pd_{1-x}Pt_x/YIG Heterostructures: Examination of Spin Relaxation Mechanism. *Phys. Rev. B: Condens. Matter Mater. Phys.* **2018**, *98*, 224424.
- (47) Zhu, L.; Ralph, D.; Buhrman, R. Spin-Orbit Torques in Heavy-Metal–Ferromagnet Bilayers with Varying Strengths of Interfacial Spin-Orbit Coupling. *Phys. Rev. Lett.* **2019**, *122*, 077201.
- (48) Chen, Y.-T.; Takahashi, S.; Nakayama, H.; Althammer, M.; Goennenwein, S. T.; Saitoh, E.; Bauer, G. E. Theory of Spin Hall Magnetoresistance. *Phys. Rev. B: Condens. Matter Mater. Phys.* **2013**, *87*, 144411.
- (49) Haney, P. M.; Lee, H.-W.; Lee, K.-J.; Manchon, A.; Stiles, M. D. Current Induced Torques and Interfacial Spin-Orbit Coupling: Semiclassical Modeling. *Phys. Rev. B: Condens. Matter Mater. Phys.* **2013**, *87*, 174411.
- (50) Chen, C.; Idzerda, Y.; Lin, H.-J.; Smith, N.; Meigs, G.; Chaban, E.; Ho, G.; Pellegrin, E.; Sette, F. Experimental Confirmation of the X-Ray Magnetic Circular Dichroism Sum Rules for Iron and Cobalt. *Phys. Rev. Lett.* **1995**, *75*, 152.
- (51) Hrabec, A.; Gonçalves, F.; Spencer, C.; Arenholz, E.; N'Diaye, A.; Stamps, R.; Marrows, C. H. Spin-Orbit Interaction Enhancement in Permalloy Thin Films by Pt Doping. *Phys. Rev. B: Condens. Matter Mater. Phys.* **2016**, *93*, 014432.
- (52) Qiu, X.; Narayanapillai, K.; Wu, Y.; Deorani, P.; Yang, D.-H.; Noh, W.-S.; Park, J.-H.; Lee, K.-J.; Lee, H.-W.; Yang, H. Spin–Orbit-Torque Engineering via Oxygen Manipulation. *Nat. Nanotechnol.* **2015**, *10*, 333–338.
- (53) Nistor, C.; Balashov, T.; Kavich, J.; Rizzini, A. L.; Ballesteros, B.; Gaudin, G.; Auffret, S.; Rodmacq, B.; Dhesi, S.; Gambardella, P. Orbital Moment Anisotropy of Pt/Co/AlO_x Heterostructures with Strong Rashba Interaction. *Phys. Rev. B: Condens. Matter Mater. Phys.* **2011**, *84*, 054464.
- (54) Isasa, M.; Villamor, E.; Hueso, L. E.; Gradhand, M.; Casanova, F. Temperature Dependence of Spin Diffusion Length and Spin Hall Angle in Au and Pt. *Phys. Rev. B: Condens. Matter Mater. Phys.* **2015**, *91*, 024402.
- (55) Onoda, S.; Sugimoto, N.; Nagaosa, N. Intrinsic versus Extrinsic Anomalous Hall Effect in Ferromagnets. *Phys. Rev. Lett.* **2006**, *97*, 126602.
- (56) Sinitsyn, N. Semiclassical Theories of the Anomalous Hall Effect. *J. Phys.: Condens. Matter* **2008**, *20*, 023201.
- (57) Sagasta, E.; Omori, Y.; Isasa, M.; Gradhand, M.; Hueso, L. E.; Niimi, Y.; Otani, Y.; Casanova, F. Tuning the Spin Hall Effect of Pt from the Moderately Dirty to the Superclean Regime. *Phys. Rev. B: Condens. Matter Mater. Phys.* **2016**, *94*, 060412.
- (58) Wang, L.; Wesselink, R.; Liu, Y.; Yuan, Z.; Xia, K.; Kelly, P. J. Giant Room Temperature Interface Spin Hall and Inverse Spin Hall Effects. *Phys. Rev. Lett.* **2016**, *116*, 196602.
- (59) Pai, C.-F.; Ou, Y.; Vilela-Leão, L. H.; Ralph, D.; Buhrman, R. Dependence of the Efficiency of Spin Hall Torque on the Transparency of Pt/Ferromagnetic Layer Interfaces. *Phys. Rev. B: Condens. Matter Mater. Phys.* **2015**, *92*, 064426.
- (60) Yu, X.; Wilhelm, O.; Moser, H. O.; Vidyaraj, S. V.; Gao, X.; Wee, A. T.; Nyunt, T.; Qian, H.; Zheng, H. New Soft X-Ray Facility SINS for Surface and Nanoscale Science at SSSL. *J. Electron Spectrosc. Relat. Phenom.* **2005**, *144*, 1031–1034.
- (61) Yu, X.; Chi, X.; Wee, A.; Rusydi, A.; Breese, M. A Scripting LabVIEW Based Program for Experiment Automation in Synchrotron Radiation Applications. *Rev. Sci. Instrum.* **2019**, *90*, 103902.